Computational Materials Science 109 (2015) 49–55

Contents lists available at ScienceDirect

Computational Materials Science

journal homepage: www.elsevier.com/locate/commatsci

Effects of nanobuds and heat welded nanobuds chains on mechanical behavior of carbon nanotubes

Xueming Yang [a,b,*], Longjie Wang [a], Yanhui Huang [a], Albert C. To [c], Bingyang Cao [b,*]

[a] Department of Power Engineering, North China Electric Power University, Baoding 071003, China
[b] Key Laboratory for Thermal Science and Power Engineering of Ministry of Education, Department of Engineering Mechanics, Tsinghua University, Beijing 100084, China
[c] Department of Mechanical Engineering and Materials Science, University of Pittsburgh, PA 15260, USA

ARTICLE INFO

Article history:
Received 27 March 2015
Received in revised form 30 June 2015
Accepted 4 July 2015

Keywords:
Nanobuds
Fullerene
Carbon nanotube
Molecular dynamics
Mechanical properties

ABSTRACT

This study reports an investigation on the effects of nanobuds and heat welded nanobuds chains (C_{60} chains attached or embedded on the surface of a SWCNT) on the mechanical properties of carbon nanotubes by molecular dynamics (MD) simulations. The bond order change and the stress concentration in the distorted connection area of nanobuds when C_{60} attaches to the surface of the SWCNT are first studied. Then the effect of multiple randomly scattered and attached C_{60} fullerenes on the ultimate tensile strength of SWCNT is discussed. It is found that both nanobuds and heat welded nanobuds chains lower the ultimate tensile strength of individual defect-free SWCNT. However, the mean post-peak strength of the CNT (after necking) is significantly enhanced by heat welded nanobuds chains. Moreover, the ultimate tensile strength of the SWCNT with vacancy defects does not decrease by heat welded nanobuds chains; interestingly, the maximum tensile strength of the SWCNTs bundles with inter-tube bridging and vacancy defects even can be enhanced by more than 20% by heat welded nanobuds chains.

1. Introduction

Fullerenes and carbon nanotubes (CNTs) have attracted a great deal of attention due to their unique physical and chemical properties [1–8]. Experimental and theoretical studies have shown that fullerenes and CNTs can be combined into nanobuds by covalently bonding fullerenes to the outer wall of carbon nanotubes, and nanobuds exhibit properties of both CNTs and fullerenes [9–14]. Nanobuds can be used as molecular anchors to prevent slipping of SWNTs in composites, thus improving the composite's mechanical properties [9]. Additionally, nanobuds possess high emission characteristics and are promising for the development of new types of vacuum electronic devices [9,12]. In recent years, the properties of nanobuds have been extensively studied, including their structures [15–18], electronic properties [19–20], chemical properties [21–24], thermal transport properties [25], magnetic properties [26] and mechanical property [14,19]. Our recent study also showed that nanobuds can promote heat welding of carbon nanotubes and SWCNTs independent of their diameters can be welded together via nanobuds even at a temperature below 1500 K [27].

It is well-known that point defects on carbon nanotubes adversely affect their mechanical properties in general, and thus nanobuds with embedding configuration should lower the stiffness and strength of carbon nanotubes. However, it should be different for nanobuds with attaching configuration where both the structure of fullerene and carbon nanotube in one nanobud are defect-free [28]. We have reported the effect of bombardment formed nanobuds with attaching configuration on the tensile strength of carbon nanotube [14], however the bombardment formed nanobuds with attaching configuration is not so typical because their distortion and stress concentration in the connection area between C_{60} and the SWCNT by collision are generally more serious than those nanobuds synthesized by chemical functionalization or formed by applying pressure [27]. More importantly, how the nanobuds with attaching configuration affect the tensile strength of carbon nanotubes is not fully understood at present, and how multiple attached C_{60} molecules or nanobuds chain with attaching configuration will affect the tensile strength of carbon nanotubes still need to be investigated.

Based on the above discussion, this paper has examined the tensile strength of SWCNTs with nanobuds or nanobuds chain with attaching configuration formed by applying pressure. A series of

* Corresponding authors.
E-mail addresses: ncepub@hotmail.com (X.M. Yang), caoby@mail.tsinghua.edu.cn (B.Y. Cao).

http://dx.doi.org/10.1016/j.commatsci.2015.07.005
0927-0256/

molecular dynamics (MD) simulations are conducted to test how the nanobuds or nanobuds chain with attaching configuration will affect the tensile strength of carbon nanotubes. First, nanobuds with attaching configuration formed by applying pressure are investigated for their effect on the tensile strength of SWCNTs; the bond order change and the stress concentration in the distorted connection area of nanobuds when C_{60} attaches to the surface of the SWCNT are studied, and the effect of multiple randomly scattered and attached C_{60} fullerenes on the ultimate tensile strength of SWCNT is discussed. Then, the effects of heat welded nanobuds chain on the tensile strength of CNT with or without defects are also presented and discussed in details. In the following works, the temperatures for getting the mechanical behavior of SWCNT are 300 K.

2. Effects of individual Nanobud with attaching configuration on the Mechanical Behavior of SWCNT

Different from the C_{60} bombardment formed nanobuds with attaching configuration, the configuration and the electronic structures of the nanobuds formed by applying pressure are more similar to those synthesized by chemical functionalization. The simulation method of the nanobuds formation by applying pressure has been described in details in our previous works [27] and will be employed in this work as well. In the simulations, the initial distance between C_{60} and single-walled CNT (SWCNT) is set to a certain value ranging from 0.8 to 1.6 Å which is less than the van der Waals distance of 3.4 Å, and thus the effect is similar to applying a pressure to make the C_{60} and CNT close. Since no constraints are set, any atoms are free to move during the simulations. If interlinking bonds between C_{60} and CNT form, the structures will equilibrate at 300 K in 0.2 ns with a fixed timestep 0.5 fs using the Nosé–Hoover thermostat. Four typical nanobuds A, B, C and D with respective number of interconnected bonds 1, 3, 4 and 5 as formed by applying pressure with the attaching configuration are shown in Fig. 1. The details of the configuration of the nanobuds in which the atoms of the interconnected bonds in both tubes and C_{60} are highlighted in yellow color as shown in Fig. 2.

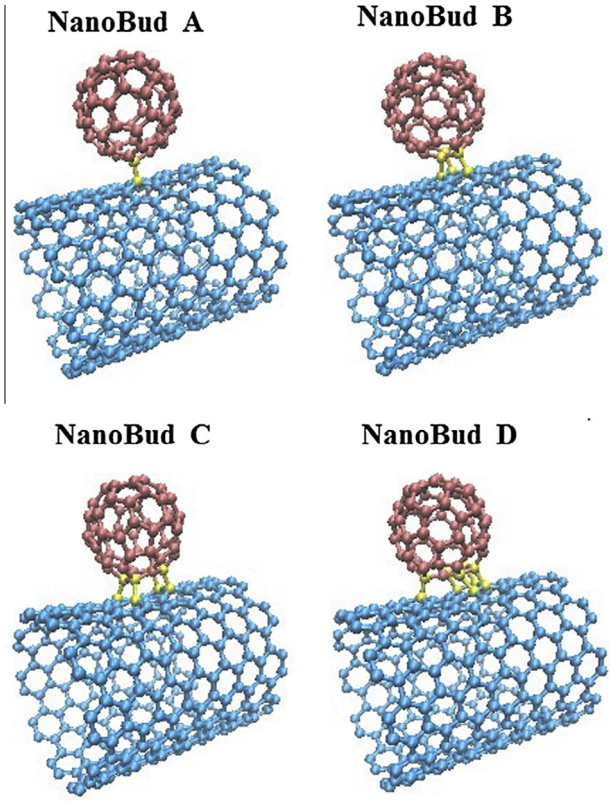

Fig. 1. Typical nanobuds with attaching configuration formed by applying pressure.

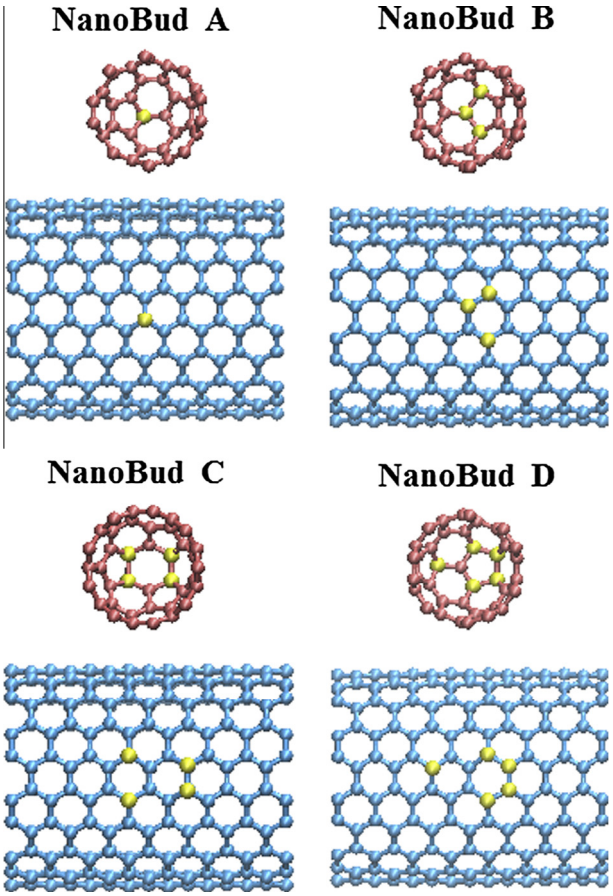

Fig. 2. Pattern of the atoms involved in the formation of the different nanobuds.

The second generation Reactive Empirical Bond Order (REBO) potential proposed by Brenner [29], which has been used widely to study the mechanical behavior of various carbon nanostructures, is employed in our MD simulations. In the MD simulations,

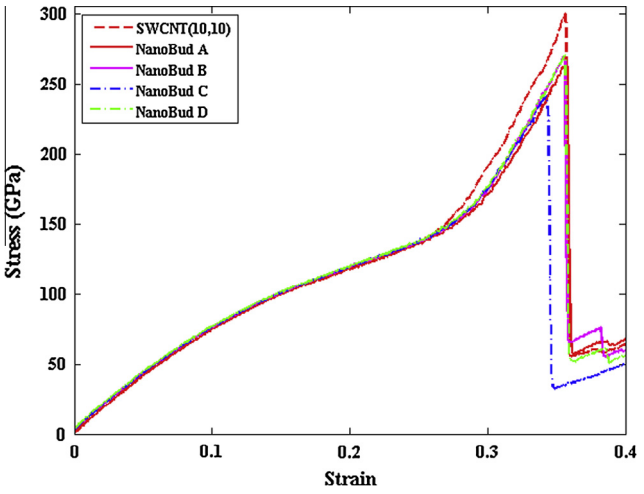

Fig. 3. Tensile stress versus strain relationships for a defect free CNT (10, 10) with or without nanobud with attaching configuration.

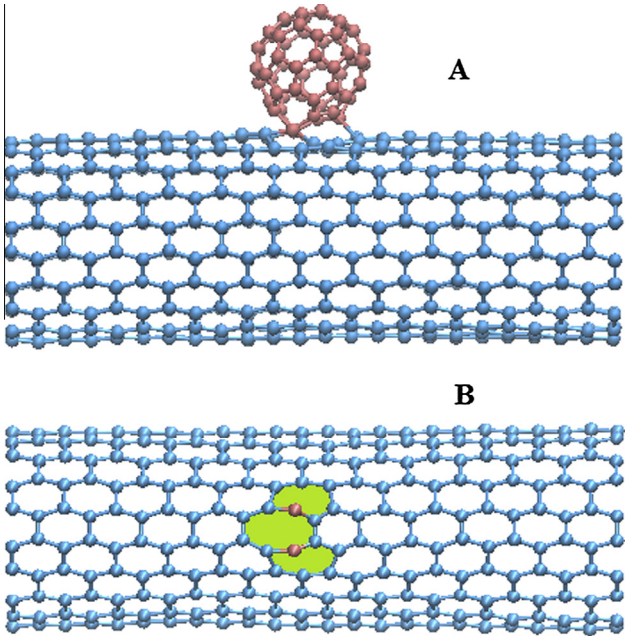

Fig. 4. Simulation slide that two atoms of C_{60} cut into the tube and defects start to appear on the tube in the tensile process of SWCNT with nanobud C: (a) front view; (b) top view of the SWCNT with the atoms of the C_{60} embeded.

Table 1
Bond length and bond order of the bonds in the distorted connection area of SWCNT (1, 1).

	Bond length	Standard deviation of bond length	Bond order	Standard deviation of bond order
SWCNT with NanoBud A	1.5038	0.004837	1.12888	0.013401
SWCNT with NanoBud B	1.5137	0.033026	1.10417	0.090057
SWCNT with NanoBud C	1.5137	0.042662	1.10657	0.109936
SWCNT with NanoBud D	1.5227	0.048395	1.08360	0.129988
SWCNT (10, 10)	1.42		1.3826	

the length of the open SWCNT (10, 10) is about 4.9 nm (20 axial period length), and the wall thickness of a SWCNT is taken as 3.4 Å [30,31]. Simulation time step is set to be 0.5 fs. Following the optimal scheme 2 (S2) described in Ref. [32], the first layers of atoms on both ends of a CNT are held rigid and all atoms except the boundary ones rigidly held are attached to a Nose–Hoover thermostat in the MD simulations of the loading process.

The stress–strain curves for a defect free SWCNTs (10, 10) with or without nanobuds attaching on the surface under uniaxial tensile strain are shown in Fig. 3. The calculated absolute values of Young's moduli for a perfect (10, 10) armchair nanotube is 0.796 TPa which is closed to the values in Refs. [30,33], and the ultimate tensile stress of SWCNT (10, 10) is 300.1 GPa which is in good agreement with the results in Ref. [32], in which the wall thickness of a SWCNT is taken as 3.4 Å. It is obvious that all the nanobuds with attaching configuration will lower the ultimate tensile strength of the SWCNT. For nanobud A, B, C and D by applying pressure, the ultimate tensile strengths decease by 12.0%, 10.3%, 19.7% and 10% comparing with a pristine SWCNT, however the values of Young's moduli changes very small, which decease by 0.29%, 0.67%, 1.32%, 2.0% comparing with a pristine SWCNT. Here the mechanical properties of the nanobuds should be directly related to their configuration. As an example, in our simulation, the atoms of the nanobuds A, B, and D are not embedded into the tubes in the

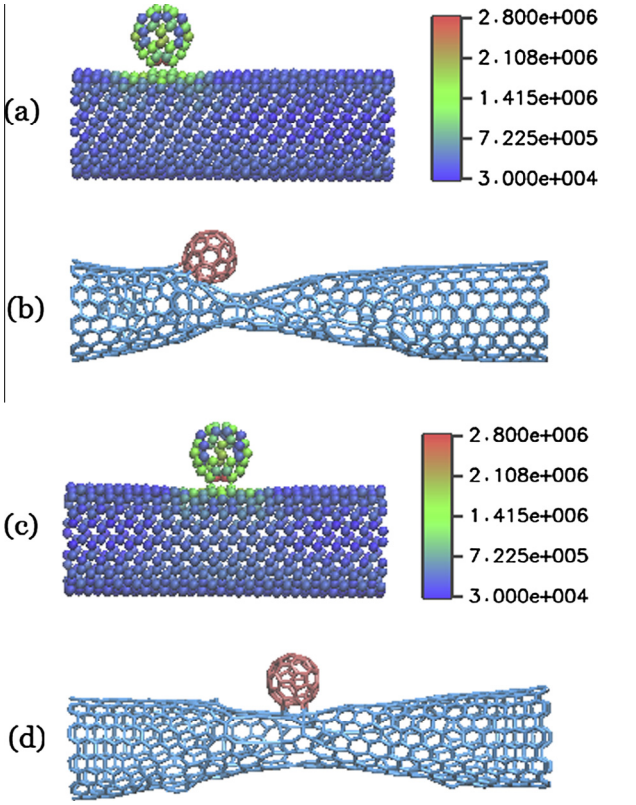

Fig. 5. The stress distribution and typical tensile state when a C_{60} attaches on the surface of SWCNT (10, 10): (a) The stress distribution at initial configuration (a C_{60} is placed at 1/3 of the CNT length); (b) typical tensile state during plastic yielding (a C_{60} is placed at 1/3 of the CNT length); (c) The stress distribution at initial configuration (a C_{60} located at middle of the CNT); (d) typical tensile state during plastic yielding (a C_{60} located at the middle of the CNT).

tensile process, and the interconnected bonds of nanobuds D cross two hexagons in the tube, which has a little consolidation effect to some extent. However, in the special case of nanobud C, as shown in Fig. 4, its two atoms will cut into the tube and one octagon and two heptagon defects appear on the tube, which accelerate the fracture of the tube and lower the ultimate tensile strength. This

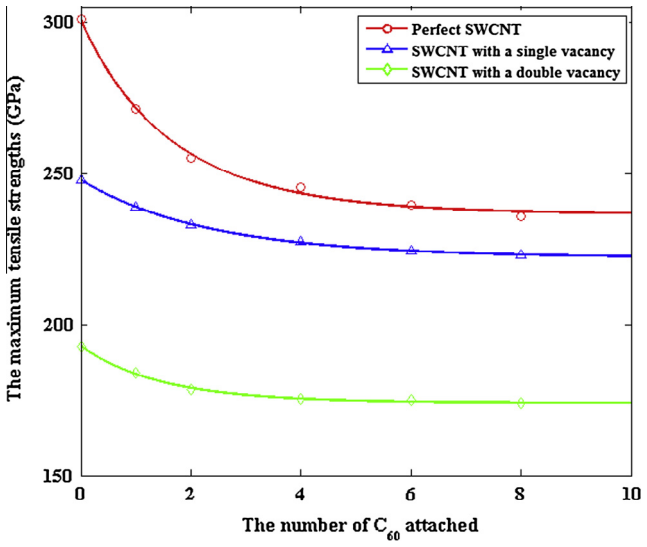

Fig. 6. The effect of multiple attached C_{60} molecules on the tensile strength of SWCNT (10, 10).

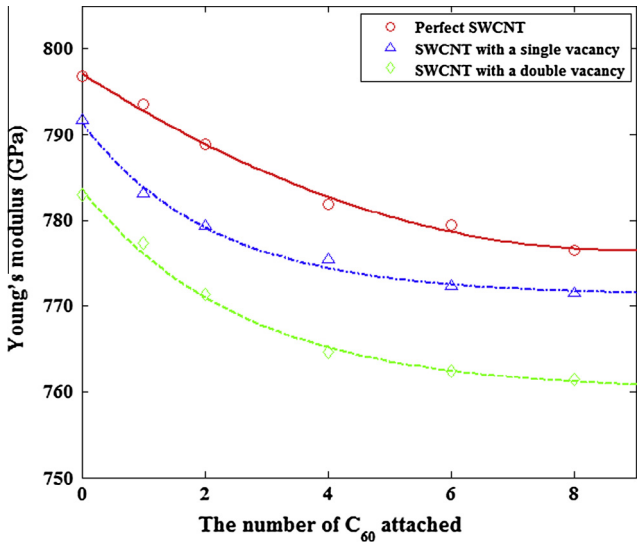

Fig. 7. The effect of multiple attached C_{60} molecules on the Young's moduli of SWCNT (10, 10).

can explain why type C is the weakest one and type D is the stiffest one.

In fact, when C_{60} attaches to the surface of the SWCNT, the curvature of the SWCNT causes the local structure around the attached C_{60} to distort. Such distortion leads to change of bond length and bond order of the bonds in the distorted connection area of SWCNTs For nanobuds A, B, C, D, the bond length and bond order of the bonds in the distorted connection area of SWCNT (1, 1) are shown in Table 1, the method for calculation of the carbon–carbon bonds order is based on an empirical equation, fitted to DFT calculations and described in [34].

In Table 1, it can be seen that, for all the carbon nanotube nanobuds with the attaching configuration, the bond order of the bonds in the distorted connection area of SWCNTs is reduced when comparing with a pristine SWCNT, which should correspond to the reduction of the tensile strength of the SWCNT attached with nanobuds.

In addition, the stress concentration appears in the distorted connection area between C_{60} and the SWCNT when C_{60} attaches to the surface of the SWCNT; in turn, the stress concentration influences its dynamic behavior in the tensile process of the SWCNT. Take an example, Fig. 5(a) and (c) show the stress distribution of each atom in the system when a C_{60} is placed at 1/3 or 1/2 of the CNT length, respectively. It can be seen that the stress concentration is obvious in the distorted connection area between C_{60} and the SWCNT before the tensile process starts. Here the stress of each atom is calculated using the vector sum of components of the per-atom stress tensor in x, y, z direction and is in units of (bars $*$ Angstrom^3) because the volume of an individual atom is not well defined or easy to compute in a deformed solid or a liquid. We find generally the plastic deformation will start, which is followed by necking near the distorted connection area between C_{60} and the SWCNT in a typical tensile process of SWCNT with nanobud, as shown in Fig. 5(b) and (d). Because the chemical bonds within the junction area between the C_{60} and SWCNT are preloaded by the presence of C_{60} attached, with the application of external tensile force on the tube ends, the C_{60} affected region becomes the weakest point and will serve as a damage nucleation site for progressive failure.

Similarly, for a perfect SWCNT, when C_{60} molecules scatter and attach on the surface of CNT, the ultimate tensile strength of SWCNT will also be lowered based on the above discussion. However, one concern may be if the strength of the SWCNT will be seriously worsened when more C_{60} molecules scatter and attach on the surface of CNT. To address this point, the effect of multiple attached C_{60} molecules on the tensile strength of SWCNT is studied. SWCNT (10, 10) with 1, 2, 4, 6, 8 C_{60} molecules random scattering on the surface of CNT with attaching configuration of nanobuds B are calculated. In each case, simulations are repeated 4 times with different C_{60} molecules random distribution. As shown in Figs. 6 and 7, the same trend is observed for SWCNT with or without vacancy that the effect of attached C_{60} molecules on the ultimate tensile strength and Young's moduli of SWCNT becomes smaller with the increase in the number of attached C_{60} molecules.

3. Effects of heat welded nanobuds chain on the mechanical behavior of individual SWCNT with defects

C_{60} molecules in nanobuds with attaching configuration can slip on the tubes, and become trapped and combined with other C_{60}

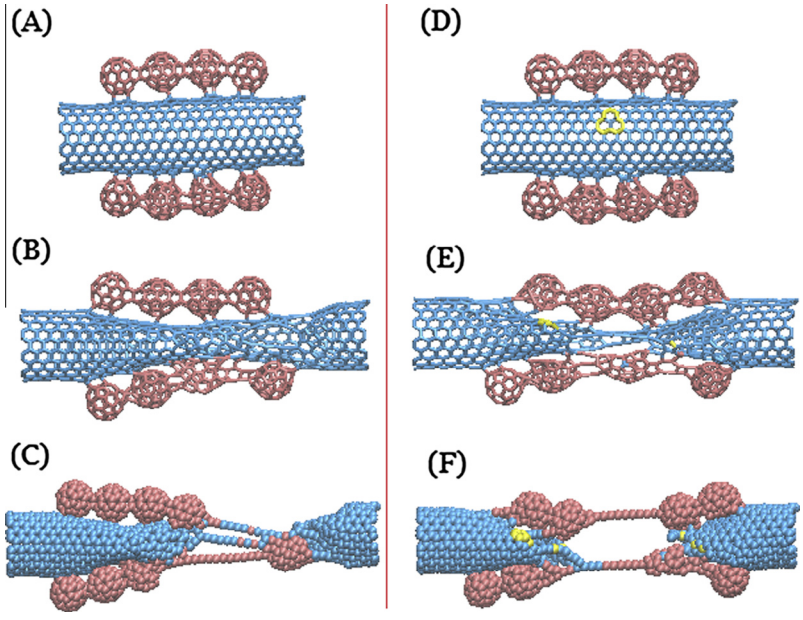

Fig. 8. Initial configuration and a typical tensile state of CNT (10, 10) with or without a single vacancy defect with two nanobuds chains

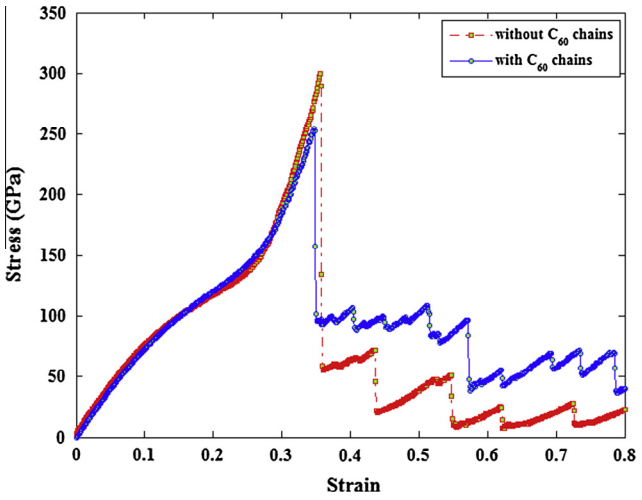

Fig. 9. Tensile stress versus strain relationships for a defect free CNT (10, 10) with or without nanobuds chain with attaching configuration.

molecules attached to the CNTs at elevated temperature, thus forming chains of C_{60} fullerenes [27].

When C_{60} chains attach on the surface of CNT, both the C_{60} chain and each C_{60} molecule will be involved in the tensile process, thus making the tensile behavior of SWCNT different. To understand how the C_{60} chains will affect the mechanical behavior of SWCNTs, the tensile stress versus strain relationships for SWCNT with or without defects will be investigated.

Here we will only consider the simplest case, in which two C_{60} chains attached on the surface of a SWCNT (10, 10) along the tube direction with or without vacancy defects. The details of simulation method of heat welding for CNTs or C_{60} chains has been described in our previous works [27,35–37] and will be employed here as well. Here first by the contact method [27], the C_{60} fullerenes are attached in a straight line along the upper and lower surface of the CNT, and then ends of the (10, 10) SWNTs (1.356 nm diameter) with the formed nanobuds are constrained, and the system excluding the constrained regions of CNT is heated from 300 K to a maximum temperature of 1500 K in 2 ns. The temperature is kept at the maximum temperature for 10 ns with a fixed timestep of 0.5 fs using the Nosé–Hoover thermostat. SWCNTs attached with the formed C_{60} chains by heating will then be annealed from the corresponding welding temperature to 300 K in 1 ns and will be kept at that temperature for 0.2 ns.

Fig. 8(A)–(C) show the tensile process of a perfect SWCNT (10, 10) with two C_{60} chains attaching on the surface, and Fig. 8(D)–(F) show the tensile process of a SWCNT (10, 10) with a single vacancy defect and two heat welded C_{60} chains attaching onto the CNT surface.

As shown in Fig. 8(B) and (C), in the tensile process of a perfect SWCNT (10, 10) with two C_{60} chains attached on the surface, the fullerenes are involved in the tensile deformation process of CNT. Compared with the tensile process of the perfect SWCNT without the C_{60} chains attached, the ultimate strength of the SWCNT (10,

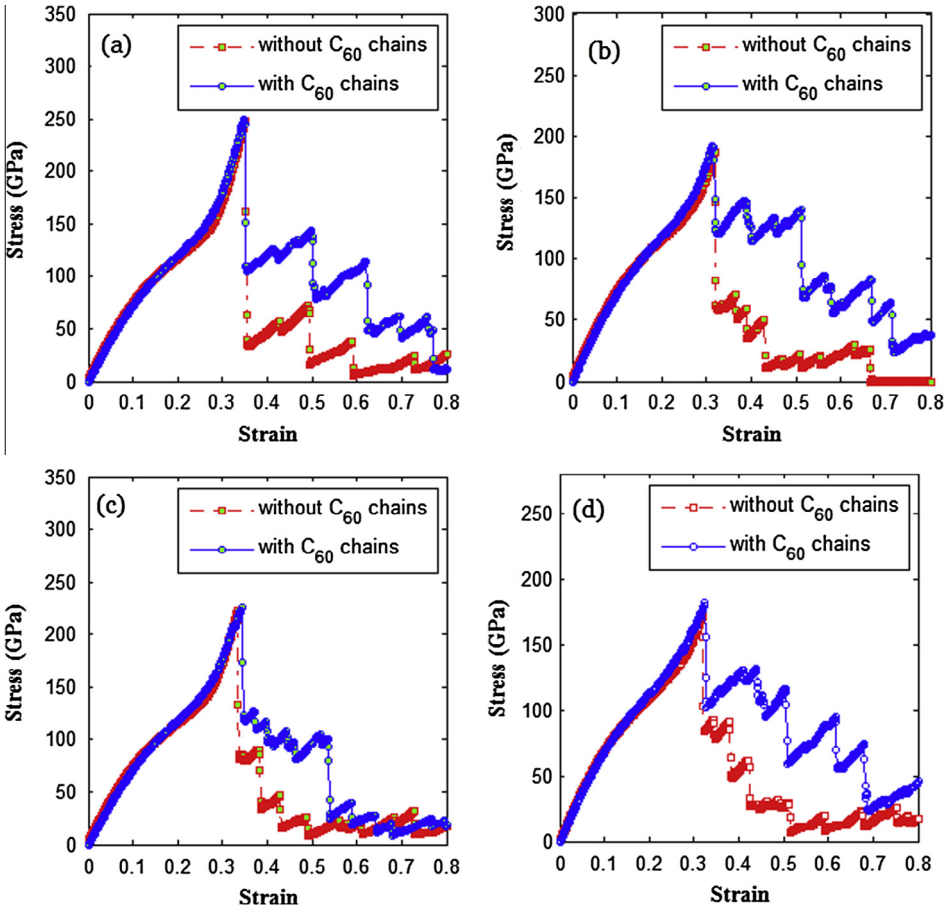

Fig. 10. Tensile stress versus strain relationships for CNT (10, 10) with or without nanobuds chain with attaching configuration: (a) CNT (10, 10) with a single vacancy defect (b) CNT (10, 10) with a double vacancy defect; (c) CNT (10, 10) with 3 random distributed single vacancy defect; (d) CNT (10, 10) with 3 random distributed double vacancy defect.

10) is reduced obviously and meanwhile the Young's moduli decrease slightly by 1.29% (with a Young's moduli value 793.5 GPa). However, the post-peak strength of the CNT (i.e. once the ultimate strength is reached) is significantly increased as shown in Fig. 9. This suggests that the degradation of the bond order by the attached C_{60} chains dominates the reduction of the ultimate strength of the SWCNT in the elastic stage. When plastic deformation starts, bond breaking occurs, followed by necking and failure of the tube. During the necking stage, the C_{60} chains provide further resistance to deformation, which causes the post-peak strength to increase. Thus the junctions between the heat welded C_{60} fullerenes and the junction between the fullerenes and SWCNT play an important role in increase of the post-peak strength and ductility of the SWCNTs, thus delaying the full fracture of the CNT.

Carbon nanotubes can have natural defects and vacancies. It is, therefore, important to know how the C_{60} chains will affect the mechanical behavior of SWCNTs with defects. Fig. 10 shows the tensile stress versus strain relationships for the defective CNT (10, 10) with or without nanobuds chains. The tensile strength of the SWCNTs (10, 10) with a single vacancy defect, a double vacancy defect, 3 random distributed single vacancy defects or 3 random distributed double vacancy defects on the surface without nanobuds chains attached are compared with the cases in which defective CNT (10, 10) attached with nanobuds chains similar to the configuration in Fig. 8(D). An interesting finding is the involvement of C_{60} chains attached in the deformation process can increase the post-peak strength and ductility of the SWCNTs in the plastic deformation stage significantly. More importantly, the ultimate strength will not be lowered. This suggests that the degradation of the ultimate strength of the SWCNTs with vacancy defects and C_{60} chains comparing with that of the perfect SWCNT is only caused by the vacancy defects.

Results show that the C_{60} chains have very little influence on the Young's moduli of SWCNTs with defects. In Fig. 10(a)–(d), the Young's modulis for the defective CNT (10, 10) with nanobuds chains are 0.7907 TPa, 0.7838 TPa, 0.7821 TPa and 0.7568 TPa, respectively, and the corresponding Young's modulis for the defective CNT (10, 10) without nanobuds chains are 0.7917 TPa, 0.7849 TPa, 0.7825 TPa and 0.7576 TPa, respectively.

4. Effects of heat welded nanobuds chain on the mechanical behavior of CNTs bundle with intertube bridging and defects

Reinforced single-walled carbon nanotube bundles by intertube bridging have been reported in Ref. [38], which showed a 30-fold increase of the bending modulus. However we found the maximum tensile strength of such SWCNT bundle will also be lowered comparing with that of the perfect SWCNT due to the interconnected bonds between the tubes, which can be observed by comparing Figs. 9 and 11(b). It also can be observed from Fig. 11(b) that the C_{60}s chains attached will not decrease the maximum tensile strength of the defect-free carbon nanotubes bundles obviously. It indicates that the interconnected bonds between the tubes

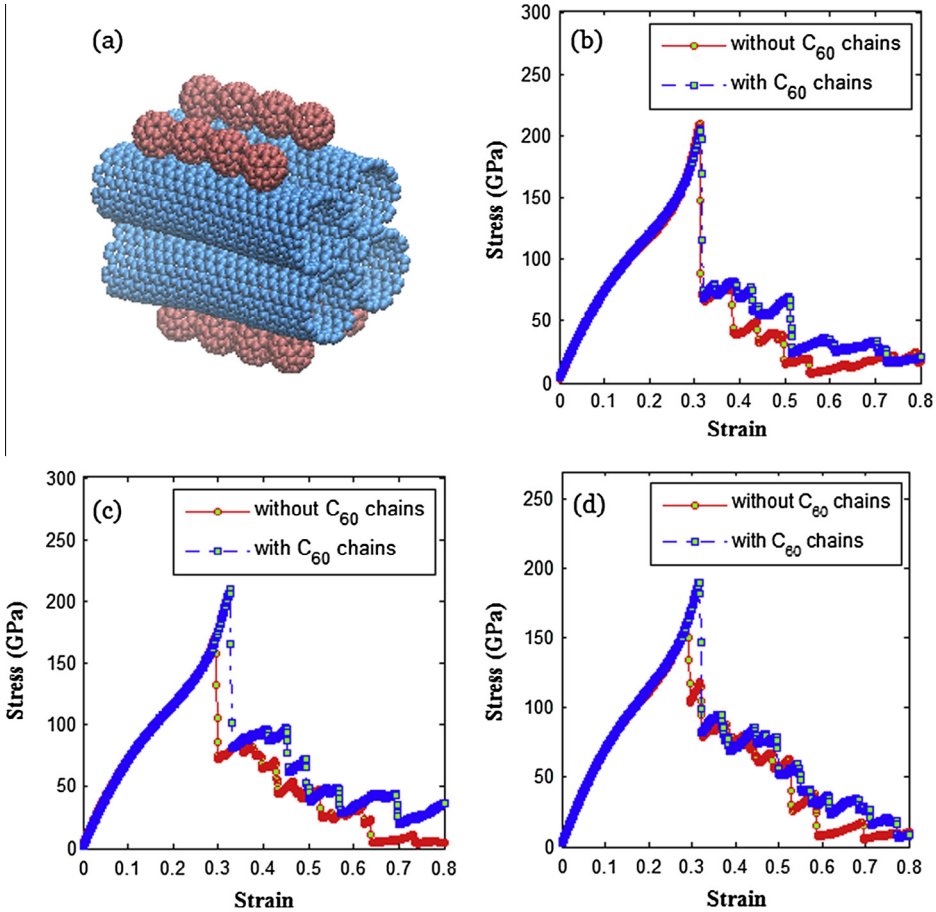

Fig. 11. Tensile stress versus strain relationships for 2 × 2 SWCNT (10, 10) bundle with or without nanobuds chains: (a) and (b) 2 × 2 SWCNT (10, 10) bundle (c) 2 × 2 SWCNT (10, 10) bundle with 3 random distributed single vacancy defects on each tube (d) 2 × 2 SWCNT (10, 10) bundle with random distributed 1 single vacancy defect and 2 double vacancy defects on each tube.

in the bundle should be responsible for the degradation of the ultimate strength of the SWCNTs bundle with C_{60}s chains attached comparing with that of the perfect individual SWCNT.

Fig. 11(c) and (d) show the tensile stress versus strain relationships for 2×2 CNTs (10, 10) bundle with or without nanobuds chains on the surfaces; in Fig. 11(c) there are 3 random distributed single vacancy defects on each tube; in Fig. 11(d) there are randomly distributed 1 single vacancy defect and 2 double vacancy defects on each tube. With C_{60}s chains attaching, the maximum tensile strength of CNTs bundle with vacancy defects can even be enhanced by 23.4% and 15.8% for the cases in Fig. 11(c) and (d), respectively. For SWCNT with vacancy defect and C_{60} chains, the vacancy defected region becomes the weakest point in general, and the C_{60} chains can act as the patch on the SWCNT. Though C_{60} chains attaching on the SWCNTs also will result in bond reduction and local stress concentration, the consolidation effect of the C_{60} chains dominates the tensile process of the SWCNTs bundle with vacancy defects.

Similarly, results also show that the C_{60} chains have very little influence on the Young's moduli of SWCNTs bundles. In Fig. 11(b)–(d), the Young's modulis for the SWCNTs bundles with nanobuds chains are 0.7823 TPa, 0.7613 TPa and 0.7496 TPa, respectively; and the corresponding Young's modulis for the SWCNTs bundles without nanobuds chains are 0.7881 TPa, 0.7649 TPa and 0.7548 TPa, respectively.

5. Conclusions

In summary, the MD simulation approach has been adopted to investigate the effects of the nanobuds on the mechanical properties of carbon nanotubes. The key results are summarized below:

Not only scattered C_{60} molecules but also C_{60} chains attached on the surface of individual perfect SWCNT would lower the ultimate tensile strength and Young's moduli of the tube, and the bond order reduction and the stress concentration in the distorted connection area of nanobuds when C_{60} attaches to the surface of the SWCNT is likely to be responsible for the reduction of the ultimate tensile strength and Young's moduli of individual SWCNT.

However, when C_{60} chains attach on the surface of individual CNT, the mean post-peak strength of the CNT after necking is significantly increased. Moreover, the C_{60} chains attaching can consolidate the SWCNT bundles with vacancy defects. Our results show that when C_{60} chains are attached, the maximum tensile strength of CNTs bundle with vacancy defects can be enhanced by more than 20%.

Nanobuds are new hybrid nanomaterials with extraordinary properties. To utilize them in engineering applications, it is necessary to predict and model their behavior under different situations [39–41]. In this study, our results have shown clearly how the tensile strength of SWCNT varies with nanobuds or nanobuds chain. It should be noted that here we only consider a simple configuration of the C_{60} chains and their attaching modes in the investigation, in which two heat welded C_{60} chains attached to the surface of a SWCNT (10, 10) lie in straight lines along the tube direction. In fact, the configuration of the C_{60} chains should be more complex in practice. Moreover, both the configurations of the C_{60} chains and the junction between the C_{60} fullerenes and SWCNT may affect the results. Therefore, how exactly the mechanical properties of carbon nanotubes will be affected by these factors still need to be further investigated.

Acknowledgments

This research is supported by the Natural Science Foundation of Hebei Province of China (Grant No. E2014502042) and the National Natural Science Foundation of China (Grant Nos. 51136001, 51356001 and 51322603).

References

[1] H.W. Kroto, J.R. Heath, S.C. O'Brien, R.F. Curl, R.E. Smalley, Nature 318 (1985) 162–163.
[2] S. Iijima, Nature 354 (1991) 56–58.
[3] X.M. Yang, D.C. Chen, Z.H. Han, X.S. Ma, A.C. To, Int. J. Heat Mass Trans. 70 (2014) 803–810.
[4] A.T. Celebi, M. Kirca, C. Baykasoglu, A. Mugan, A.C. To, Comput. Mater. Sci. 88 (2014) 14–21.
[5] V. Vijayaraghavan, C.H. Wong, Comput. Mater. Sci. 89 (2014) 36–44.
[6] S.J. Guo, Q.S. Yang, X.Q. He, K.M. Liew, Comput. Mater. Sci. 85 (2014) 324–331.
[7] Á. Varga, M. Pfohl, N.A. Brunelli, et al., Phys. Chem. Chem. Phys. 15 (37) (2013) 15470–15476.
[8] M.E. Snowden, M.A. Edwards, N.C. Rudd, J.V. Macpherson, Phys. Chem. Chem. Phys. 15 (2013) 5030–5038.
[9] A.G. Nasibulin, P.V. Pikhitsa, H. Jiang, D.P. Brown, A.V. Krasheninnikov, A.S. Anisimov, P. Queipo1, A. Moisala1, D. Gonzalez, G. Lientschnig, A. Hassanien, S.D. Shandakov, G. Lolli, D.E. Resasco, M. Choi, D. Tománek, E.I. Kauppinen, Nat. Nanotechnol. 2 (3) (2007) 156–161.
[10] A.G. Nasibulin, D.P. Brown, P. Queipo, D. Gonzalez, H.J. Jiang, E.I. Kauppinen, Chem. Phys. Lett. 417 (2006) 179–184.
[11] A.G. Nasibulin, A.S. Anisimov, P.V. Pikhisa, H. Jiang, D.P. Brown, M. Choi, E.I. Kauppinen, Chem. Phys. Lett. 446 (1) (2007) 109–114.
[12] X.L. Li, L.Q. Liu, Y.J. Qin, W. Wu, Z.X. Guo, L.M. Dai, D.B. Zhu, Chem. Phys. Lett. 377 (2003) 32–36.
[13] E.F. Sheka, L.K. Shaymardanova, J. Mater. Chem. 1106 (2011) 0643.
[14] X.M. Yang, L.J. Wang, Y.H. Huang, Z.H. Han, A.C. To, Phys. Chem. Chem. Phys. 16 (2014) 21615–21619.
[15] R.J. Nicholls, J. Britton, S.S. Meysami, A.A. Koós, N. Grobert, Chem. Commun. 49 (93) (2013) 10956–10958.
[16] A. Seif, E. Zahedi, T.S. Ahmadi, Eur. Phys. J. B 82 (2) (2011) 147–152.
[17] Y. Tian, D. Chassaing, A.G. Nasibulin, P. Ayala, H. Jiang, A.S. Anisimov, E.I. Kauppinen, Phys. Status Solidi B 245 (10) (2008) 2047–2050.
[18] Y.W. Wen, X. Liu, X. Duan, R. Chen, B. Shan, Model. Simul. Mater. Sc. 21 (3) (2013) 035006.
[19] M.G. Ahangari, M.D. Ganji, F. Montazar, Solid State Commun. 203 (2015) 58–62.
[20] P. Zhao, P.J. Wang, Z. Zhang, M.J. Ren, D.S. Liu, Physica B 405 (8) (2010) 2097–2101.
[21] I.V. Anoshkin, A.G. Nasibulin, P.R. Mudimela, J. Raula, V. Ermolov, E.I. Kauppinen, Carbon 50 (11) (2012) 4171–4174.
[22] W. Koh, J.I. Choi, S.G. Lee, S.S. Jang, Carbon 49 (1) (2011) 286–293.
[23] J. Raula, M. Makowska, J. Lahtinen, A. Sillanpää, N. Runeberg, J. Tarus, E.I. Kauppinen, Chem. Mater. 22 (15) (2010) 4347–4349.
[24] X. Wang, C. Ma, K. Chen, H. Li, P. Wang, Phys. Lett. A 374 (1) (2009) 78–90.
[25] G.C. Loh, D. Baillargeat, J. Appl. Phys. 113 (12) (2013) 123504.
[26] X. Zhu, H. Su, Phys. Rev. B 79 (16) (2009) 165401.
[27] X.M. Yang, Y.H. Huang, L.J. Wang, Z.H. Han, A.C. To, RSC Adv. 4 (2014) 56313–56317.
[28] H.Y. He, B.C. Pan, J. Phys. Chem. C 113 (49) (2009) 20822–20826.
[29] D.W. Brenner, O.A. Shenderova, J.A. Harrison, S.J. Stuart, B. Ni, S.B. Sinnott, J. Phys.-Condens. Matter. 14 (2002) 783–802.
[30] G.H. Gao, T. Cagin, W.A. Goddard III, Nanotechnology 9 (1998) 184–191.
[31] J.L. Zang, Q.Z. Yuan, F.C. Wang, Y.P. Zhao, Comp. Mater. Sci. 46 (2009) 621–625.
[32] K. Mylvaganam, L.C. Zhang, Carbon 42 (10) (2004) 2025–2032.
[33] M.F. Yu, O. Lourie, M.J. Dyer, K. Moloni, T.F. Kelly, R.S. Ruoff, Science 287 (5453) (2000) 637–640.
[34] A.C.T. Van Duin, S. Dasgupta, F. Lorant, W.A. Goddard III, J. Phys. Chem. A 105 (41) (2001) 9396–9409.
[35] X.M. Yang, Z.H. Han, Y.H. Li, D.C. Chen, P. Zhang, A.C. To, Physica E 46 (2012) 30–32.
[36] N.M. Piper, Y. Fu, J. Tao, X. Yang, A.C. To, Chem. Phys. Lett. 502 (2011) 231–234.
[37] X.M. Yang, P. Zhang, Chem. Phys. Lett. 547 (2012) 42–46.
[38] K.A. Csanyi, G. Salvetat, J.P. Lee, T.N. Couteau, E. Kulik, et al., Nat. Mater. 3 (3) (2004) 153–157.
[39] J.A. Baimova, B. Liu, S.V. Dmitriev, N. Srikanth, K. Zhou, Phys. Chem. Chem. Phys. 16 (36) (2014) 19505–19513.
[40] J.A. Baimova, B. Liu, S.V. Dmitriev, K. Zhou, Phys. Status Solidi-R. 8 (4) (2014) 336–340.
[41] J.A. Baimova, E.A. Korznikova, S.V. Dmitriev, B. Liu, K. Zhou, Rev. Adv. Mater. Sci. 39 (1) (2014) 69–83.